ELSEVIER

Journal of Power Sources 93 (2001) 41–49

JOURNAL OF POWER SOURCES

www.elsevier.com/locate/jpowsour

Time-dependent BASE performance and power degradation in AMTEC

M.A.K. Lodhi[a,*], P. Vijayaraghavan[b], A. Daloglu[a]

[a]*Department of Physics, Texas Tech University, Lubbock, TX-79409, USA*
[b]*Department of Mechanical Engineering, Texas Tech University, Lubbock, TX-79409, USA*

Received 22 May 2000; accepted 11 June 2000

Abstract

During extended testing at the Jet Propulsion Laboratory and the Air Force Research Laboratory, it has been found that maximum power output of the PX-3A AMTEC cell decreases with time. Starting with a peak maximum power output of 2.45 W it decreases almost continuously to 1.27 W at the end of 18 000 h. In this paper, the factors contributing to this power loss have been investigated.

The cell uses a β″-alumina solid electrolyte (BASE) whose material degrades with time due to changes in the chemical and thermal conditions within the cell during operation. The analysis shows that the β″-alumina degradation manifests itself as an increase in its ionic resistance which reduces power output. The β″-alumina is responsible most of the power degradation in the first 7000 h of operation. Thereafter, though β″-alumina degradation continues to cause power loss, other components and their materials in the cell also contribute to power loss. Some suggestions are made that will help reduce the rate of power degradation and extend the useful and functional time of the cell which primarily deal with reducing the chemical contamination of the BASE, use of β-alumina instead of β″-alumina and keeping the electrode current density below a certain critical value.

Keywords: Power degradation; BASE; Electrode current density

1. Introduction

The alkali metal thermal electric converter (AMTEC) is being considered for use in future space missions [1–3]. It is a thermally regenerative, electrochemical device for the direct conversion of heat to electrical power. While AMTEC technology development is primarily focused on space applications, it is also expected to find many terrestrial uses. AMTECs can be used for hybrid electric vehicle systems [4–6], independent and portable power generation units [7,8], residential power generation either in conjunction with or independent of the electric grid [9], power generation for recreational vehicles, power for air-conditioning and lighting in cross country transportation, charging rechargeable batteries, running residential self-powered furnaces [10,11], for military uses [11], and micro-cogeneration [11].

The AMTEC uses a solid electrolyte made of the ceramic β″-alumina. The β″-alumina solid electrolyte (BASE), a low electronic but high ionic conductivity material [12,13], is the heart of the AMTEC and the key to its working. The PX-3A cell, which is the object of this study, is part of a series of AMTEC cells developed originally for NASA's Pluto Express Mission after whose acronym 'PX' this series is named. A schematic diagram of the PX-3A is shown in Fig. 1. The PX-3A typically works at a temperature of about 1200 K at the hot side and 600 K at the condenser. Heat is supplied from an external source to the cell by means of the hot plate. The hot plate, in turn, transfers heat to the evaporator and the BASE tubes by radiation, and conduction through the thermal rings. The evaporator converts liquid sodium to its vapor form at high pressure. The vapor passes to the interior of the BASE tubes through a port in the thermal rings. The inside of the BASE tube, thus, is in contact with high-pressure sodium vapor. This side is covered with a TiN anode and the outside with a TiN cathode. Metal (molybdenum) mesh current collectors are laid over both the cathode and the anode. The high pressure of sodium vapor inside the BASE tubes causes electrochemical expansion of sodium through the BASE after ionization. The ions diffuse through the BASE toward the low-pressure side in response to the pressure differential gradient of free Gibbs energy. The sodium vapor pressure P_c at the BASE/cathode interface is given by [14]

$$P_c = P_c^{oc} + \Delta P = P_c^{oc} + \sqrt{\frac{2\pi R_g T_B}{M}}\left(\frac{3G}{8\pi}\right)\frac{MJ}{F} \quad (1)$$

* Corresponding author. Tel.: +1-806-742-3778; fax: +1-806-742-1182.
E-mail address: b5mak@ttacs.ttu.edu (M.A.K. Lodhi).

0378-7753/01/$ – see front matter
PII: S0378-7753(00)00537-1

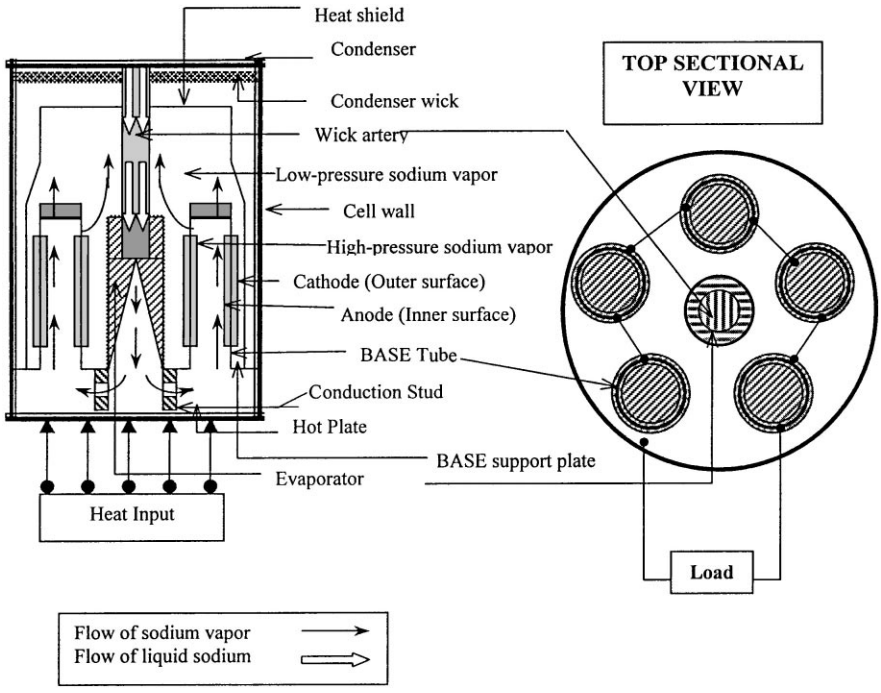

Fig. 1. Side and top sectional views of the PX-3A cell (the top sectional view shows the electrical circuit also).

where ΔP is the pressure losses through the electrode, R_g the universal gas constant (8.314 J/mol K), T_B the temperature of the BASE, G the geometric factor for pressure losses, M the molecular weight of sodium (23 g/mol), J is the electrode current density (A/m^2), F is Faraday's constant (96485 C/mol) and P_c^{oc} the sodium vapor pressure at the BASE/cathode interface in open-circuit condition is given by

$$P_c^{oc} = P_{cond}\sqrt{\frac{T_B}{T_{cond}}} \tag{2}$$

where P_{cond} and T_{cond} being the sodium vapor pressure at the condenser and the temperature of the condenser, respectively. The effective electromotive force V_0 of the cell is

$$V_0 = V^{oc} - \xi^a + \xi^c \tag{3}$$

where V^{oc} is the open-circuit voltage given by

$$V^{oc} = \frac{R_g T_B}{F}\ln\left(\frac{P_a}{P_c^{oc}}\right) = \frac{1}{f_B}\ln\left(\frac{P_a}{P_c^{oc}}\right) \tag{4}$$

where P_a is the sodium vapor pressure at the anode/BASE interface and is equal to the saturation vapor pressure at the evaporator temperature, and f_B is defined as F/R_gT_B.

The charge-exchange polarization overpotentials at the anode (ξ^a) and at the cathode (ξ^c) used in Eq. (3) are calculated using the following expression in which, the 'x' in the subscripts may be substituted by either 'a' for anode or 'c' for cathode:

$$\xi_x = -\frac{2}{f_B}\ln\left\{\frac{1}{2}\left[\left(\frac{J_x}{J_x^o}\right)^2 + 4\frac{P_x}{P_x^{oc}}\right]^{1/2} + \frac{1}{2}\frac{J_x}{J_x^o}\right\} \tag{5}$$

where $J_c = J$ at the cathode and $J_a = -J$ at the anode, and J_x^o the exchange current density and is a measure of the nature of the contact at the BASE/electrode interface and is related to the saturation equilibrium exchange current density as

$$J_x^o = J_0^o\left[\frac{P_x^{oc}}{P_{sat}(T_B)}\right]^a \tag{6}$$

J_0^o in Eq. (6) is a function of the BASE temperature and of the type of electrode. It can be expressed as

$$J_0^o = B\frac{P_{sat}(T_B)}{\sqrt{T_B}} \tag{7}$$

where B is the temperature-independent exchange current (A K$^{1/2}$/Pa m^2), and P_{sat} is the saturation pressure of sodium vapor at BASE temperature.

Electrical leads in contact with the porous electrodes exit through the wall of the device and are connected to an external load. The electrons flow from the anode, through these leads, the external load and reach the cathode, where they recombine with the sodium ions that have passed through the BASE and form low-pressure sodium vapor. This low-pressure vapor flows to the condenser where it is converted to liquid sodium. PX-3A uses a condenser with a micromachined surface. This condenser ensures the formation of a continuous film of liquid sodium (which has high reflectivity) that helps reduce parasitic heat losses by reflecting radiation from the hot end of the cell back to that end. Liquid sodium flows through drainage groves in the condenser to a drainage artery. This artery causes the liquid sodium to flow to the capillary wick that returns the liquid

sodium back to the evaporator by capillary action. The PX-3A uses a circumferential heat shield to reduce heat losses. The shield intercepts a part of the radiation from the hot end to the cold end and reflects it back to the hot end thus reducing radiation losses. The evaporator converts the liquid sodium to vapor at high pressure and this cycle is repeated for the continuous production of electrical power [15–19].

2. Role of the BASE in power degradation

The β-alumina family of ceramics has a unique property of conduction among solid electrolytes. Unlike many other electrolytes, β″-alumina (a member of this family) is a poor conductor of electrons but is a very good conductor of ions [12,13]. This unique conduction property of β″-alumina is primarily due to its crystal structure. Since the BASE is so crucial to AMTEC, any change in its properties will most certainly affect power output. Changes in its properties will manifest themselves as a change in ionic resistance and will thus affect power output. There are many mechanisms in which changes occur in the material and/or internal structure of the BASE which in turn cause BASE resistance and hence power output to change.

The working temperature of the BASE is around 1000 K. The BASE is subjected to this high temperature in sodium vapor environment, which is highly reactive and corrosive at high temperatures, for long time exposure. The BASE undergoes two main changes [20], namely, thermal breakdown and chemical contamination, which affect the BASE performance in several ways discussed in these broad categories.

2.1. Thermal breakdown

Thermal breakdown can occur at AMTEC working temperatures. This involves more than one process and occurs over a few 1000 h. While a certain process may itself not cause power degradation to any significant extent it can add to the overall cumulative effect. There are several modes in which thermal breakdown can occur and these are described below.

2.1.1. Loss of sodium as sodium oxide

Sodium ions present in the conduction plane of β″-alumina are responsible for ionic conduction. Any loss of sodium from the structure will result in decrease in ionic conductivity [21]. Kennedy and Sammells studied sodium content and conductivity as a function of MgO doping level. Their work established that BASE resistivity depends on sodium content. It was found that the optimum concentration of sodium (that gave minimum resistivity) depended on MgO content. As the MgO content increases, the optimum sodium content also increases [22]. For instance, the variation of resistivity with sodium content of β″-alumina containing 2% MgO is in the form of a parabola with the minimum resistivity occurring at roughly 7.5% of sodium content. This process of sodium loss takes place at a slow rate and its effect may not be evident for a few 1000 h [23,24]. However, when long time spans are considered even a slow process such as this will affect the performance of the BASE.

2.1.2. Formation of molten dendrites

Dendrites are columns of material different from the rest of the material in phase, composition and/or microstructure. In this case, molten sodium dendrites are formed within the structure due to both the high temperature and flow of charge. As these dendrites increase in size and propagate through the structure, they can ultimately cause an electrical short between the cathode and the anode causing electrons to flow directly from the anode to the cathode thus reducing the amount of charge flowing through the external circuit [22].

2.1.3. Crack formation

This is a mechanical failure but influences power generation. A crack is a void or discontinuity in a material that has a propensity to grow or increase in size causing the material to finally rupture and fail. Richman and Tennenhouse, and Tennenhouse et al. have studied degradation of β″-alumina and conclude that cracks form when Na^+ ions migrate through the ceramic and are converted to metallic Na [22]. Their postulated mechanism consists of ceramic dissolution at pre-existing surface cracks, which results in selective removal of electrolyte from crack tips. The process can be described as follows. Microcracks at the β″-alumina surface are filled with sodium. When the cell starts to generate power, sodium formation results at the tips of the microcracks and the cracks propagate into the electrolyte as a result of the pressure caused by sodium flow out of the crack. The presence of excess sodium on the fracture surface of β″-alumina from a cell which failed in operation was detected by electron spectroscopy in support of the proposed failure mechanism that sodium ion migration leads to intergranular weakening and fracture [22,25]. Crack formation is detrimental to the performance of the cell because of the following. If the crack propagates through the thickness of the BASE tube, a short or opening is created between the high-pressure sodium and low-pressure sodium regions of the cell. This will cause some of the high-pressure sodium to flow in the atomic state directly to the low-pressure region through the crack due to the pressure differential without ionizing at the anode. Since it is the ionization of metallic sodium at the anode that results in the formation of ions and their subsequent flow through the external load to the cathode, any reduction in the number of electrons formed at the anode will cause a reduced current to flow to the external load and hence, reduced power output.

2.1.4. Changes in microstructure

Polycrystalline β″-alumina consists of crystals of different orientations giving it a grain microstructure. A grain is an individual crystal in a polycrystalline material. It is known

that high temperatures and sufficiently long periods of time cause grain growth. Grain growth is defined as an increase in the size of grains when adjacent crystals are broken and become part of a single crystal [26]. Grain growth can affect ionic conductivity adversely. As grain size increases (total material volume is conserved), the density of grains decreases and contact between the grains in the BASE and the electrode, decreases [27,28] thus decreasing the exchange current. The exchange current is the reversible oxidation–reduction reaction at the BASE-electrode interface and refers to the ionization reactions leading to the formation of Na^+ ions and reformation of Na atoms. Decrease in exchange current reduces the number of electrons formed due to ionization. Another effect of grain growth is on electrical resistance. Grain growth reduces the number of grains or grain boundaries in a given region that an ion traveling through that region encounters. Hence, the ion experiences a reduced resistance (because, the larger the number of grain boundaries that an ion crosses the more resistance it encounters). On the other hand, the coalescence of grains over a few 1000 h may also cause microscopic voids in the material thereby greatly increasing resistance to ion transport. However, the latter effect being more pronounced than the former, this actually increases the BASE ionic resistance as a net result of grain growth [27,28].

2.2. Chemical contamination

The cell wall and many other components in the cell are made of stainless steel. High-pressure sodium vapor at high temperature in contact with these components reacts with stainless steel and/or cause corrosion leading to escape of elements like chromium and manganese from stainless steel. The products of these reactions will then enter the sodium stream and either deposit on the surface of the BASE or enter the material itself [27–30]. Surface-deposition of these reactants blocks the pores in the BASE and obstruct the flow of the sodium vapor. When these reactants enter the material itself, they may deposit on grain boundaries and increase grain boundary resistance. They may also substitute Na^+ ions in the conduction layer of the BASE crystal [31]. This is detrimental to conductivity especially if the atomic sizes of these impurities are more than that of sodium. Bigger ions than sodium will result in slower ionic motion and hence, lesser ionic conductivity. Also, because the width of the conduction layer in the rombohedral structure of β''-alumina is only about 0.4 nm, larger ions may be obstructed in their flow [27,30]. Besides these reactants, contaminants in the BASE like $NaAlO_2$ also have a deleterious effect on ionic conductivity, mechanical strength and chemical stability.

3. Modeling of BASE performance

The metallurgical, mechanical, thermophysical and chemical changes in the BASE material discussed above occur with the passage of time during the cell operation. While some of the changes affect BASE resistance directly, others reduce power output either by reducing the current flowing through the external load or likewise. The effect of all these changes is simulated as an increase in the ionic resistance through the BASE. Hence, an empirical relation between BASE ionic resistance and time has been developed. In this work, attention is only focused on the change in BASE ionic resistance. This does not, however, imply that other components do not undergo any change.

The BASE ionic resistance is given by [14]

$$R_B = \rho_B t_B \tag{8}$$

where R_B is the ionic resistance of the BASE, ρ_B the ionic resistivity of the BASE and t_B the thickness of the BASE tube.

The Joule heating (Q_J) in each of the leads is given by [14]

$$Q_J = \frac{I\sqrt{\lambda}}{\sin(\delta)}(T_B + T_{cond})[1 - \cos(\delta)] \tag{9}$$

where λ ($= 2.45 \times 10^{-8}$ W Ω/K^2) is the Franz–Lorenz number, T_B the temperature of the BASE tube, T_{cond} the temperature of the cold end (condenser) and

$$\delta = \frac{\sqrt{\lambda}}{k}\frac{L}{A_l}I \tag{10}$$

where L is the length of one conductor lead, k the thermal conductivity of the lead material, A_l the cross-sectional area of the lead and I the total cell electric current. The net power output is given by

$$P_{out} = VI = \frac{V^2}{R_{load}} \tag{11}$$

where R_{load} is the load resistance, and the load voltage (V) is calculated as

$$V = N_s[V_0 - (R_B + R_{cont})J] - 2\frac{Q_J}{JA_E} \tag{12}$$

where N_s is the number of BASE tubes in a multi-tube AMTEC cell, R_{cont} the internal resistance of the cell, J the electrode current density, A_E the electrode area on one BASE tube, Q_J the Joule heating in one lead and V_0 the effective cell electromotive force.

From Eq. (12), it can be seen that any change in BASE ionic resistance (R_B) directly affects the load voltage which in turn affects the power output.

As a first step, an empirical expression for BASE resistance as a function of time is determined to generate a power versus time characteristic similar to the observed power degradation. In order to develop this empirical model, assuming that no changes occur in the properties of other components, it is necessary to vary BASE resistance as a function of time which generates a set of data that shows the value of BASE resistance at each interval of time where the observed data for power degradation were taken. A regression analysis is performed on the data set thus obtained to

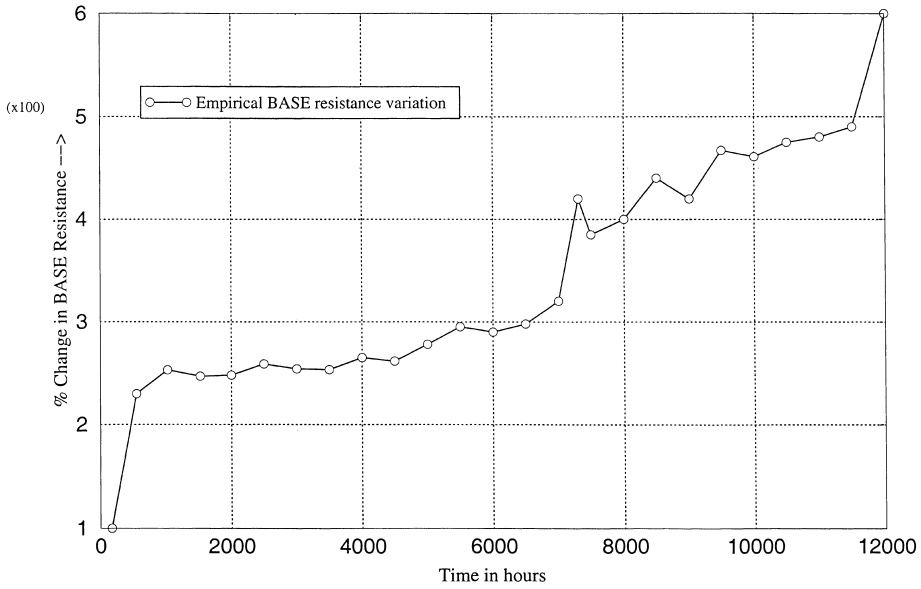

Fig. 2. Empirical variation of BASE resistance that results in obserbed power degradation.

look for a function that will describe BASE resistance change with time. This analysis is done using the statistical and plotting package XMGR on a Linux platform [32].

The variation of BASE resistance with time thus obtained, shown in Fig. 2, represents the change in total internal resistance of the cell simulating the effect of all the components and materials in the cell. A regression analysis is performed on this variation to obtain a suitable expression. Fig. 3 shows the results of this regression analysis using exponential, logarithmic and power functions (see Eqs. (13)–(15). To test the validity of the empirical variation in BASE resistance obtained (Fig. 2), these functions are incorporated in the program by multiplying the functions with the expression that calculates BASE resistance in the program. The program is then made to run and it is found that the variation shown in Fig. 2 gives power–time characteristics very close to the observed power degradation. The curve fits used only reflect the relative change in BASE resistance. To obtain the absolute values of the BASE resistance, it is assumed that the entire tube has the same resistance throughout. The BASE resistance variations used in Fig. 3 are as follows:

$$\text{Exponential fit}: \quad R_{\text{base}} = 0.71 \times \text{e}^{(9\times10^{-5}\times\text{time})} \tag{13}$$

$$\text{Power fit}: \quad R_{\text{base}} = 0.05 \times \text{time}^{0.374} \tag{14}$$

$$\text{Logarithmic fit}: \quad R_{\text{base}} = -1.98 + 0.393 \times \ln(\text{time}) \tag{15}$$

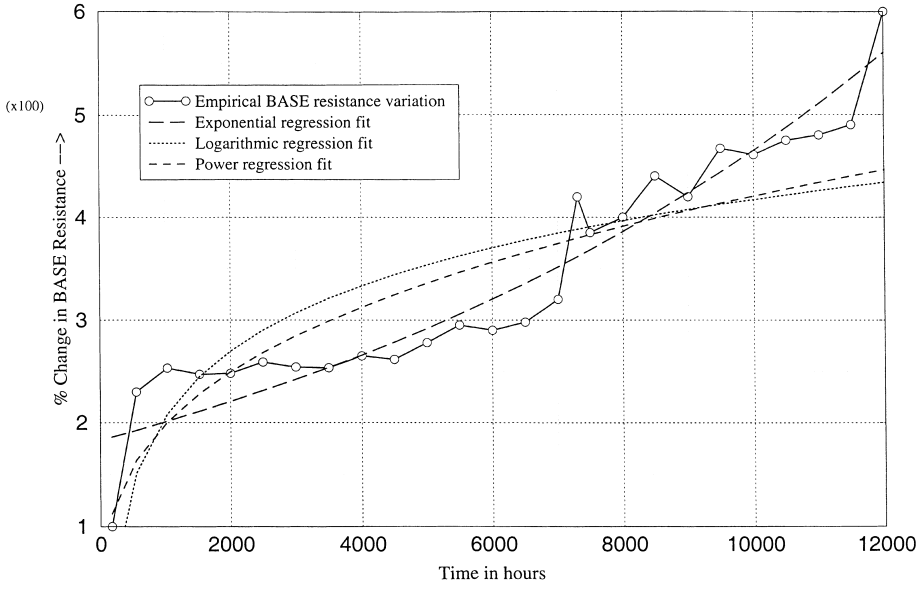

Fig. 3. Exponential, logarithmic and power regression fits for empirical BASE resistance variation.

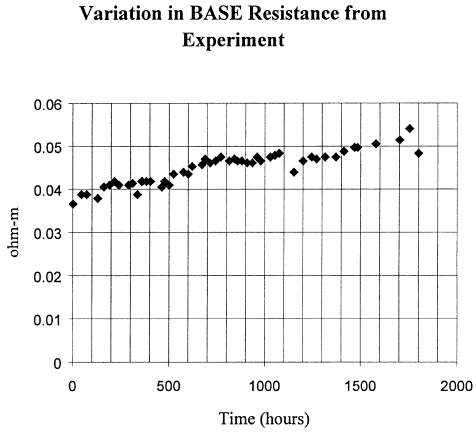

Fig. 4. Experimentally observed variation in BASE resistivity with time.

Williams et al. [33] have conducted experiments to study the change in β″-alumina's ionic resistivity with time. The β″-alumina in the experiments is exposed to a sodium vapor environment with the temperature and pressure conditions similar to those in an AMTEC. As shown in Fig. 4, β″-alumina's ionic resistivity shows a gradual increase over 1800 h. Fig. 5 shows a comparison of the empirical BASE resistance variation and the experimentally observed one in terms of percentage change. As can be seen, the actual values are less than the empirical. This is only to be expected because the empirical values represent the total internal resistance of the cell and not just of the BASE which of course will be lower than the total resistance. The effect of change in the resistance of the BASE alone on power is shown in Fig. 6. This is done, as before, by fitting the experimental data to a function using regression analysis. The change in BASE resistivity with time is expressed as percentage change and is fit to a linear function given by the

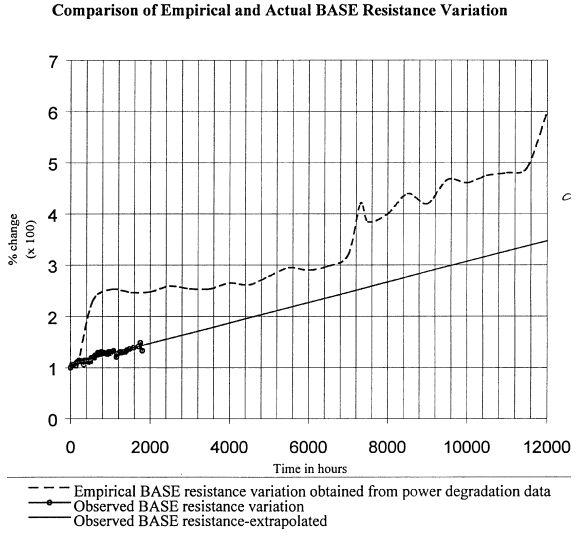

Fig. 5. Comparison of empirical variation in BASE resistance with experimentally observed variation.

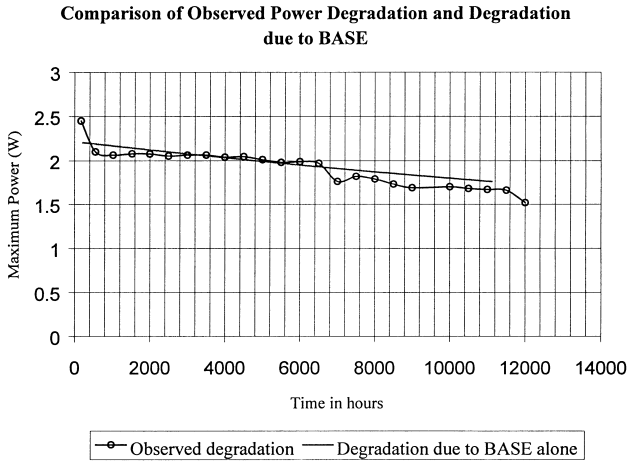

Fig. 6. Comparison of actual power degradation and the degradation caused by the BASE alone.

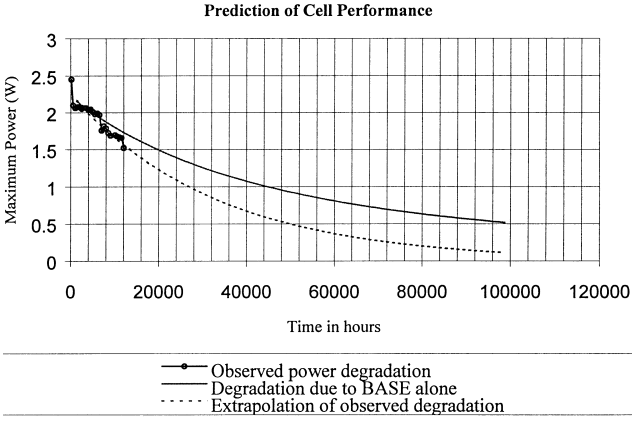

Fig. 7. Extrapolated results of the observed power degradation and that due to the BASE alone.

equation of the form

$$y = 0.0002x + 1.0713 \quad (16)$$

where y is the percentage change in BASE resistivity, and x the time in hours.

This extrapolation is shown in Fig. 5 for 12000 h compared with the empirical variation. It can be seen from Fig. 6 that power degradation due to the BASE alone matches closely with the observed power degradation for up to about 7000 h. Beyond this point, observed degradation is more than that due to the BASE alone. This phenomenon is seen magnified in Fig. 7, which also shows the relative effect of the BASE on power degradation but extrapolated to 100 000 h.

4. Conclusions

We have seen that the AMTEC performance mainly depends on BASE resistance. This analysis shows that at

the start of operation almost all of the internal resistance is due to the BASE. However, at the end of 12 000 h, the BASE resistance is about 57.8% of the total internal resistance (see Fig. 5). Similarly, the BASE is indeed responsible for practically all of the power degradation for the first 7000 h or so (see Fig. 6). After this initial match between observed power degradation and that due the BASE alone, the effect of changes in the properties of other components begins to contribute to the overall degradation as the continuously increasing separation between the two curves suggests. At the end of 100 000 h, projected power loss from observed data as a percentage of initial value is 92.1%, while percentage power loss due to the BASE degradation alone is 75.9%. Both of these support the conjecture of this study that the BASE is responsible to a significant extent and is indeed a major cause of power degradation. For slowing down the power degradation in the PX-3A, we make the following observations.

4.1. Reducing the chemical contamination of the BASE

The Cr^{3+} ions present in stainless steel are corroded away from stainless steel by the action of sodium and enter the crystal structure of β″-alumina, they can be particularly detrimental to the BASE. The β″-alumina is particularly unstable in the presence of trivalent ions [22,34]. To prevent these contaminants from reaching the BASE, some ionic or other kinds of filters should be used. This is feasible for terrestrial applications but may not be so for space missions.

4.2. Possible use of β-alumina instead of β″-alumina

The β″-alumina is stabilized by doping it with lithium or magnesium oxides. But these dopants are detrimental to electrolyte life. β-alumina is stable without doping and hence may be used in place of β″-alumina. However, β-alumina has lower ionic conductivity than β″-alumina. To counter this problem, single crystal β-alumina may be used which has higher conductivity than polycrystalline β-alumina [22]. Polycrystalline β-alumina may also be used and a process of sintering and annealing can be applied to increase its conductivity.

4.3. Avoiding causes of structural instability of β″-alumina

Lithium oxide adversely affects BASE stability. A threshold current density at which the breakdown occurs can be predicted by a β″-alumina degradation model developed by Richman and Tennenhouse [22]. This has also been observed experimentally. For instance, β″-alumina containing 1.1 wt.% Li_2O can be charged to less than 200 mA/cm^2, while β″-alumina containing 0.25 wt.% Li_2O can be charged up to less than 1 A/cm^2 before degradation occurs [22]. For every chemical and metallurgical configuration/composition of the BASE, and system conditions, there is a certain critical current density below which there is no electrolyte degradation but above which degradation occurs. Above the critical current density, rate of BASE degradation increases with increase in current density. Therefore, it is suggested that the critical current density be determined for the configuration of the cell under consideration and efforts be made to maintain the current density below this critical value without compromising on system performance. If this is not possible, and it is necessary for the current density to be higher than the critical value, it may be kept as close to the critical value as possible because the higher the current density above the critical value, the higher will be the rate of BASE degradation and hence, power degradation.

Acknowledgements

This work is supported in parts by the United States Air Force Office of Scientific Research via Sub-contract no. F99-0832 CFDA 12800, Grant no. 98-0001 and the Texas Higher Education Coordinating Board Grant no. ATP 003644-091.

Appendix A.

There is another dopant that affects BASE stability that is discussed here. In doping β″-alumina with lithium or magnesium, the Li^+ or Mg^{2+} ions take up some of the Al^{3+} positions crystal structure. However, these dopants are detrimental to the life of the BASE. Fig. 8 shows the relative structural stability of the different members of the β-alumina family [22]. As can be seen, stability depends on both Na_2O and MgO content. Change in the content of any one can

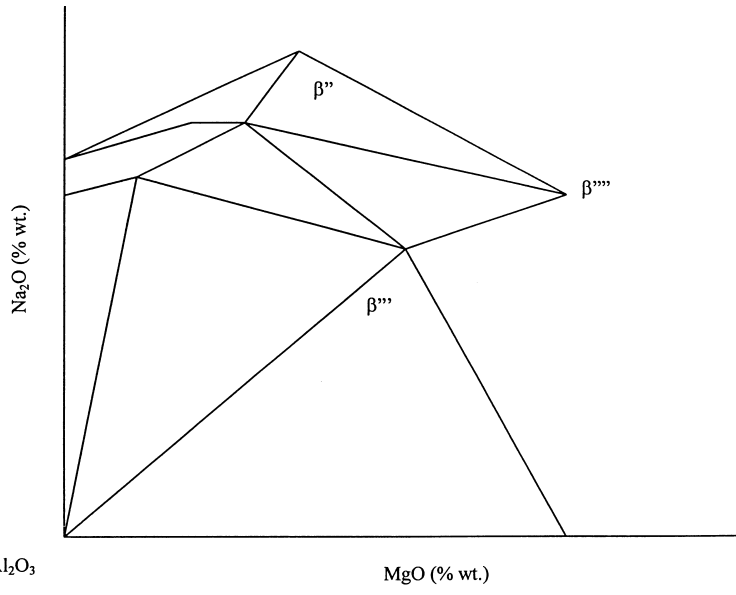

Fig. 8. Dependence of structural stability of the β-aluminas on relative amounts of MgO and Na_2O.

upset the balance and cause β″-alumina to become less stable. For instance, at a certain amount of MgO, there is a range of Na_2O composition for which β″-alumina is stable. If the Na_2O content falls outside this range, β″-alumina will become unstable. Since, sodium oxide depletion from β″-alumina occurs over extended periods of time, the MgO content in β″-alumina should be adjusted so that β″-alumina remains in the region of stability corresponding to that MgO content in spite of this loss of sodium oxide.

References

[1] M.E. Carlson, J.C. Giglio, R.K. Sievers, Design and fabrication of multi-cell AMTEC power systems for space applications, in: Proceedings of the American Institute of Physics Conference 0094-243X, Issue 420, Number 3, 1998.

[2] A. Schock, H. Noravian, C. Or, V. Kumar, Recommended OSC Design and analysis of AMTEC power system for outer-planet missions, in: Proceedings of the American Institute of Physics Conference 0094-243X, Issue 158, Number 2, 1999.

[3] J.F. Ivanenok, R.K. Sievers, R.B. Harty, G. Johnson, Conceptual design of a 500 W solar AMTEC space power system, in: Proceedings of Intersociety Energy Conversion Engineering Conference, Conf. 30, Vol. 1, 1995.

[4] T.K. Hunt, R.K. Sievers, J.F. Ivanenok, Low emission AMTEC automotive power system, in: Proceedings of Intersociety Energy Conversion Engineering Conference 0146-9555X, Conf. 30, Vol. 3, 1995.

[5] T. Hunt, R. Sievers, J. Ivanenok, AMTEC auxiliary power unit for hybrid electric vehicles, in: Proceedings of Intersociety Energy Conversion Engineering Conference, Conf. 29, Vol. 3, 1994.

[6] R. Mital, R.K. Sievers, T.K. Hunt, Ultra clean burner for an AMTEC system suitable for hybrid electric vehicles, in: Proceedings of Intersociety energy Conversion Engineering Conference, Conf. 32, Vol. 2, 1997.

[7] R. Mital, T.J. Hendricks, R.C. Svedberg, R.K. Sievers, Propane fueled AMTEC auxiliary electric power systems for remote site deployment, American Society of Mechanical Engineering Publications — Advanced Energy Systems Division, Vol. 37, 1997.

[8] J.F. Invanenok, R.K. Sievers, 20–500 W AMTEC auxiliary electric power system, in: Proceedings of Intersociety Energy Conversion Engineering Conference 0146-955X, Conf. 31, Vol. 4, 1996.

[9] T.K. Hunt, J.F. Ivanenok, R.K. Sievers, AMTEC power systems for remote site applications, in: Proceedings of American Institute of Physics Conference 0094-243X, Issue 324, 1995.

[10] J.F. Ivanenok, R.K. Sievers, AMTEC powered residential furnace and auxiliary power, in: Proceedings of Intersociety Energy Conversion Engineering Conference, Conf. 31, Vol. 2, 1996.

[11] R. Mital, R.K. Sievers, J.R. Rasmussen, T.K. Hunt, Performance evaluation of gas-fired AMTEC power systems, International Gas Research Conference, Vol. 4, 1998, pp. 917–928, Gas Research Institute, 1998.

[12] H. Sato, Some theoretical aspects of solid electrolytes, Topics in Applied Physics (Solid Electrolytes), Springer, Berlin, New York, 1977.

[13] D.R. Treadwell, A.C. Sutorik, S.S. Neo, R.M. Laine, R.C. RSvedberg, Synthesis of beta-alumina polymer precursor and its pyrolysis to ultrafine beta-Al_2O_3 powders, in: Proceedings of Intersociety Energy Conversion Engineering Conference, Vol. 2, 1997.

[14] Jean-Michel Tournier, Mohammed S. El-Genk, Michael Schuller Paul Hausgen, An Analytical Model for Liquid-Anode and Vapor-Anode AMTEC Converters, in: Proceedings of the 14th Symposium on Space Nuclear Power and Propulsion, 2nd Space Technology and Applications International Forum held in Albuquerque, NM, 1997, American Institute of Physics, AIP Conference Proceedings no. 387, III, pp. 1543–1552.

[15] R.K. Sievers, J.E. Pantolin, R.C. Svedberg, D.A. Butkiewicz, C.A.C. Borkowski, A.C. Huang, T. J. Hendricks, T.K. Hunt, Series II AMTEC cell design and development, in: Proceeedings of Intersociety Energy Conversion Engineering Conference, Vol. 2, 1997.

[16] A. Schock, H. Noravian, C. Or, Coupled thermal, electrical, and fluid flow analyses of AMTEC converters, with illustrative application to OSC's cell design, in: Proceeedings of Intersociety Energy Conversion Engineering Conference, Conf. 32, Vol. 2, 1997.

[17] A. Schock, H. Noravian, C. Or, V. Kumar, Design, analysis, and fabrication procedure of AMTEC cell, test assembly, and radioisotope power system for outer-planet missions, in: Proceedings of the 48th International Astronautical Congress, Turin, Italy, 1997.

[18] J.F. Ivanenok, R.K. Sievers, W.W. Schultz, Modeling of remote condensing AMTEC cells, in: Proceedings of American Institute of Physics Conference 0094-243X, Issue 301, 1994.

[19] A. Yamada, H. Tsukuda, T. Hashimoto, H. Kikuchi, Experimental study on AMTEC using sodium-vapor-fed cells, in: Proceedings of the Intersociety Energy Conversion Engineering Conference, Conf. 29, Vol. 2, 1994.

[20] M. Steinbrueck, V. Heinzel, F. Huber, W. Peppler, Behavior of beta-alumina solid electrolytes in an AMTEC environment, Liquid Metal Systems Journal, Number 2, 1995.

[21] R.M. Williams, M.A. Ryan, M.L. Homer, L. Laura, K. Manatt, V. Shields, R.H. Cortez, J. Kulleck, The thermal decomposition of sodium beta-alumina solid electrolyte ceramic in AMTEC Cells, Meeting Abstracts — Electrochemical Society — All Divisions — 1091-8213, Number 1, 1998, p. 831, Electrochemical Society 1998.

[22] J.H. Kennedy, The beta-aluminas, Topics in Applied Physics — Solid Electrolytes, Springer, Berlin, New York, 1977.

[23] R.M. Williams, M.A. Ryan, M.L. Homer, L. Laura, K. Manatt, V. Shields, R.H. Cortez, J. Kulleck, The thermal decomposition of sodium beta-alumina solid electrolyte ceramic in AMTEC cells, Meeting Abstracts — Electrochemical Society — All Divisions — 1091-8213, Number 1, 1998, p. 831, Electrochemical Society 1998.

[24] R.M. Williams, M.A. Ryan, W. Phillips, Loss of alkali oxide from beta-alumina and its importance to AMTEC life issues, in: Proceedings of 32nd Intersociety Energy Convention Engineering Conference, 1997, American Institute of Chemical Engineers, 1997.

[25] W. Fischer, High energy batteries with solid sodium ion conductive electrolytes, High Conductivity Solid Ionic Conductors-Recent Trends and Applications, World Scientific, Singapore, Teaneck, NJ, 1989.

[26] S.H. Avner, Introduction to Physical Metallurgy, McGraw-Hill Book Co., Singapore, 1990.

[27] V. Ganesan, V. Ganesan, Corrosion of annealed AISI 316 stainless steel in sodium environment, J. Nuclear Mater. 256 (1) (1998) 69.

[28] M.A. Ryan, A. Kisor, R.M. Williams, B. Jeffries-Nakamura, D. O'Connor, Lifetimes of thin film AMTEC electrodes, in: Proceedings of the 29th Intersociety Energy Conversion Engineering Conference.

[29] D.L. Alger, Some corrosion failure mechanisms of AMTEC Cells, in proceedings of the 32nd Intersociety Energy Conversion Engineering Conference, 1997 Journal of Intersociety Energy Conversion Engineering Conference, 1997, Conf. 32, Vol. 2, pp. 1224–1229, American Institute of Chemical Engineers, 1997.

[30] G.C. Farrington, B. Dunn, J.O. Thomas, The multivalent beta-aluminas, High Conductivity Solid Ionic Conductors — Recent Trends and Applications, World Scientific, Singapore, Teaneck, NJ, 1989.

[31] M.A. Ryan, R.M. Williams, M.L. Underwood, B. Jeffries-Nakamura, D. O'Connor, Electrode, current collector and electrolyte studies for AMTEC cells, in: Proceedings of the American Institute of Physics Conference, Issue 271/2, 1993, pp. 905–912, American Institute of Physics, 1993.

[32] P. Vijayaraghavan, Power degradation and performance evaluation of BASE in AMTEC, Master's Thesis, Texas Tech University, 1999.
[33] R.M. Williams, M.A. Ryan, M.L. Homer, L. Lara, K. Manatt, V. Shields, R.H. Cortez, J. Kulleck, The thermal stability of sodium beta-alumina solid electrolyte ceramic in AMTEC cells, Space Technology and Applications International Forum, The American Institute of Physics, 1999.
[34] L. Zu-Xiang, Significance of nonstoichiometry of beta-alumina, High Conductivity Solid Ionic Conductors-Recent Trends and Applications, World Scientific, Singapore, Teaneck, NJ, 1989.